Purcell-enhanced Raman scattering from atmospheric gases in a high-finesse microcavity

Benjamin Petrak,[1] Nicholas Djeu,[2] and Andreas Muller[1,*]

[1]*Department of Physics, University of South Florida, Tampa, Florida 33620, USA*
[2]*MicroMaterials, Inc., Tampa, Florida 33637, USA*

We demonstrate the Purcell spontaneous-emission enhancement effect for Raman scattering from gases in a $\sim$10-μm-long Fabry-Pérot microcavity with a mode volume of $\sim$100 μm^3 and a peak finesse of 50 000. The cavity increases the pump laser intensity by resonant recirculation while simultaneously enhancing the rate of Raman scattering into a separate cavity mode by modification of the density of states of the intracavity electromagnetic vacuum field. The result is an overall enhancement of $\sim$10^7 compared to free-space emission into the same solid angle as the cavity, enabling trace gas sensing requiring only minute sample quantities.

I. INTRODUCTION

Purcell first observed that the presence of reflectors in the vicinity of an emitter can significantly alter its spontaneous-emission rate [1]. An emitter that in free space couples to the continuum of modes of the free-space electromagnetic field can, if properly positioned inside an optical resonator, couple to a single sharply peaked mode of the confined field. Thus, not only can most of the emitted radiation be collected into a single spatial mode (that can then be coupled, e.g., into an optical fiber), but the overall rate at which the emission occurs can also be drastically increased. This effect is now well known for the case of two-level fluorescence from atoms [2–4]. Recently, the Purcell effect has also been the subject of intensive research using solid-state microcavities in the context of single-photon generation for quantum communication applications [5–7].

Its ubiquity in fluorescence measurements notwithstanding, the Purcell effect has been studied much less for the case of Raman scattering. Milestone experiments include the investigation of spontaneous Raman emission enhancement in liquids using planar resonators [8] as well as in solids using planar [9,10] and ring resonators [11,12], but not in gases. This is despite its usefulness for a variety of sensing applications such as medical diagnostics, hazardous materials detection, industrial process monitoring, and air quality control, for which its notoriously weak gas scattering cross section of only order 10^{-31} cm^2/sr is a severe drawback. There have been many attempts to overcome this limitation of Raman scattering, including most notably surface-enhanced Raman scattering, in which surface plasmon interactions yield enhancements large enough to detect single molecules adsorbed onto metallic nanoparticles [13,14].

We report here the measurement of enhanced spontaneous Raman scattering from atmospheric gases by the Purcell effect in a three-dimensionally-confining optical microresonator. We take advantage of recent advances in laser microfabrication for the construction of a microcavity which combines ultrasmall mode volume, high finesse and the possibility to freely flow analytes in its interior [15–18]. We show how a double resonance condition can be achieved by which an increase in both the laser intensity and the spontaneous emission rate

_____

*mullera@usf.edu

together provide an enhancement of order 10^7 compared to free space emission. We demonstrate that with only 10 mW of input laser power at $\lambda \approx 864$ nm, Raman scattering from CO$_2$ in ambient air can be detected, involving an interaction with only millions of molecules.

II. THEORETICAL BACKGROUND

Purcell-enhanced spontaneous Raman scattering *for gases* requires an open Fabry-Pérot microcavity in which the laser couples to one cavity mode (mode number m) containing n_l laser photons and the Raman-shifted emission is coupled to another mode (mode number m') containing n_s Stokes photons. If stimulated Raman scattering is ignored ($n_s \ll 1$), the relationship between n_s and n_l is governed by the rate equation [19],

$$\frac{dn_s}{dt} = \frac{F_p}{\tau_R}n_l - n_s/\tau_c^{(s)}. \tag{1}$$

The Raman photon buildup rate per pump laser photon, F_p/τ_R, is written here as the ratio of the "Purcell factor," F_p, and the free-space spontaneous Raman "lifetime," τ_R, which is related to the familiar differential Raman scattering cross section, $d\sigma/d\Omega$, by

$$\tau_R^{-1} = \frac{8\pi}{3}\frac{\nu_l}{\nu_s}Nc\frac{d\sigma}{d\Omega}, \tag{2}$$

where N is the gas number density, c is the speed of light in vacuum, and ν_s (ν_l) is the frequency of the Stokes (laser) photons. The Stokes photon number decays at a rate $1/\tau_c^{(s)} = 2\pi\Delta\nu_c^{(s)}$, where $\Delta\nu_c^{(s)}$ is the full width at half-maximum (FWHM), in Hz, of the cavity resonance at the Stokes frequency. The Purcell factor for Raman scattering has been calculated in [10] as

$$F_p = \frac{3c}{8\pi^2}\frac{\lambda_s^2}{V}\frac{1}{\Delta\nu_R + \Delta\nu_c^{(s)}}, \tag{3}$$

which explicitly takes account of the finite spectral overlap between the cavity mode and the Raman transition line shape with linewidth $\Delta\nu_R$. Here λ_s is the wavelength of the Stokes photons. The mode volume, V, for Raman scattering in a symmetric resonator that supports Gaussian beams can be

approximated as (see Appendix A)

$$V = (\lambda_l + \lambda_s)\frac{L^2/4}{\tan^{-1}[L/\sqrt{2(R-L/2)L}]}, \quad (4)$$

where λ_l is the pump laser wavelength, L is the length of the resonator, and R is the mirror radius of curvature. In steady state, Eq. (1) provides the rate of emission out of one end of the cavity as $\gamma_{\text{cav}} = (1/2)n_l F_p/\tau_R$. As a function of the input power, P_{in}, the intracavity laser photon number is given by $n_l = 2P_{\text{in}}\tau_c^{(l)}/h\nu_l$, where $\tau_c^{(l)} = 1/(2\pi\Delta\nu_c^{(l)})$ is the cavity photon lifetime at the pump laser frequency. Thus, overall, for our experimental conditions, we get

$$\gamma_{\text{cav}} = \frac{Nc\lambda_s^3 P_{\text{in}}\tau_c^{(l)}}{\pi hV}\frac{d\sigma/d\Omega}{\Delta\nu_R + \Delta\nu_c^{(s)}} \quad (5)$$

for the rate of emission out of one end of the cavity.

The microresonator in this work enhances the flux of collected Raman-scattered photons in three different ways. First, the recirculation of the laser at a resonant frequency causes an increase in pump power by a factor of $\mathcal{F}^{(l)}/\pi$, where $\mathcal{F}^{(l)}$ is the cavity finesse at the laser frequency. Second, the rate of emission into the Stokes cavity mode is enhanced via the Purcell effect by a factor of F_p compared to the total free-space emission rate. Third, the cavity directs *all* the emission into a well-defined spatial mode of solid angle $\Delta\Omega \approx \lambda_s^2/(\pi w_0^2)$, corresponding to a factor of $4\pi^2 w_0^2/\lambda_s^2$ increase in collection efficiency compared to the same solid angle in free space. Here $w_0^2 = \lambda_s\sqrt{(R-L/2)L/2}/\pi$ [20] is the square of the beam waist of the cavity mode. Thus, overall the cavity provides an enhancement of collected Raman photons of $(\mathcal{F}^{(l)}/\pi)F_p(4\pi^2 w_0^2/\lambda_s^2)$ compared to the same solid angle in free space. Assuming $\mathcal{F}^{(l)} = 10^4$, $L = 10$ μm, $R = 50$ μm, $\Delta\nu_R + \Delta\nu_c^{(s)} = 2$ GHz, and $V = 150$ μm^3, this enhancement is of order 10^7.

III. EXPERIMENTS

To experimentally measure this effect, we use the setup depicted in Fig. 1. A microcavity was constructed with one micromirror on a planar substrate and another at the tip of a single-mode fiber [18]. Both mirrors had a radius of curvature of $R \approx 40$ μm. The cavity assembly [Fig. 1(b)] was built with a hermetical seal, and gases were delivered directly to the cavity region. We chose a rigid flexure design with mechanical amplification employing two piezoelectric actuators so that the cavity length could be varied over its entire region of stability ($L < 2R$) [20]. One actuator provided an offset and the other was used for scanning the cavity length. The cavity assembly was temperature-controlled and protected from air currents by an enclosure. One advantage of the fiber micromirror is that gases such as CO_2, with diffusion coefficients in air of order 10^{-5} m^2/s, can traverse the 62 μm distance corresponding to the fiber radius in less than a millisecond, thus enabling fast gas delivery. The pump laser beam was mode-matched into the cavity using a single aspheric lens as shown in Fig. 1(c). A Pound-Drever-Hall (PDH) lock maintained the cavity on resonance with this laser, with feedback provided to one of the piezoelectric actuators [21].

The practical and conceptual challenges in implementing the condition which makes Eq. (1) valid for gases lie in the
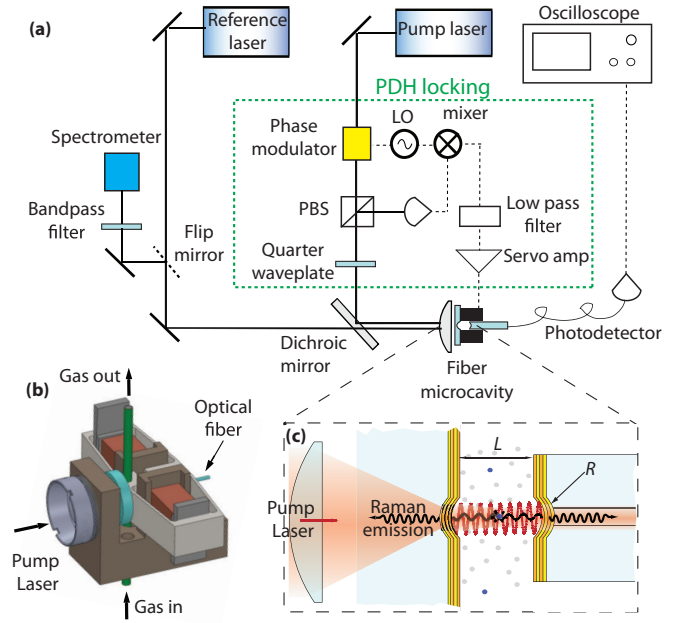
FIG. 1. (Color online) (a) The microcavity was frequency-locked to the tunable "pump" laser using the PDH scheme, consisting of a phase modulator driven by a local oscillator (LO), a polarizing beam splitter (PBS), a quarter-wave plate, and feedback electronics. The Raman-scattered emission was collected via a dichroic mirror. (b) Microcavity assembly. (c) The microcavity consisted of a micromirror on a planar substrate facing a nominally identical mirror at the tip of a single-mode fiber.

fact that, unlike in planar cavities for which angle tuning can be applied [9,10], or in larger solid resonators with a spectrally broad Raman gain medium [11,12], it is necessary to find specific cavity length and pump laser frequency pairs. Achieving this double resonance is further constrained by the finite bandwidth of high-reflectivity coatings.

For both the laser and the Raman-shifted emission to be resonant with the microcavity, one must have

$$k_l L - \Delta\varphi + \varphi_l = m\pi, \quad (6)$$

$$k_s L - \Delta\varphi + \varphi_s = m'\pi, \quad (7)$$

where k_l and k_s are the wave numbers for the laser and Stokes waves, φ_l and φ_s are the phase shifts experienced by the two waves at the mirror, and $\Delta\varphi$ is the Gouy phase shift given by

$$\Delta\varphi = \tan^{-1}(z_2/z_R) - \tan^{-1}(z_1/z_R), \quad (8)$$

where z_R is the Rayleigh range defined by the microcavity, and z_2 and z_1 (negative) are the positions of the two mirrors (so that $z_2 - z_1 = L$) [20]. The double resonance condition is given by

$$\frac{1}{2L}\left[\left(\frac{m}{n} - \frac{m'}{n'}\right) + \frac{\Delta\varphi}{\pi}\left(\frac{1}{n} - \frac{1}{n'}\right) - \frac{1}{\pi}\left(\frac{\varphi_l}{n} - \frac{\varphi_s}{n'}\right)\right]$$
$$= \Delta\bar{\nu}_V, \quad (9)$$

where n and n' are the refractive indices of air at the laser and Stokes wavelengths, and $\Delta\bar{\nu}_V$ is the Raman shift. For the cases of interest here, we have $(n' - n) \lesssim 10^{-7}$ and the second
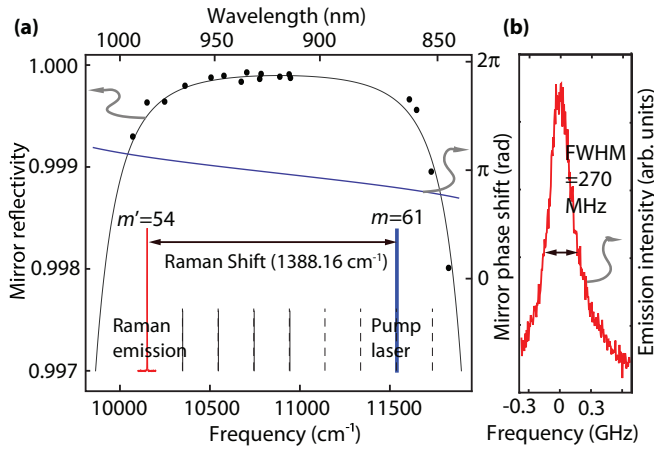
FIG. 2. (Color online) (a) Mirror reflectivity obtained from a measurement of the microcavity finesse as a function of wavelength. At the maximum reflectivity ($\lambda \approx 920$ nm) the cavity finesse is $\approx 50\,000$. The experimental (theoretical) cavity resonances are represented by the solid (dashed) vertical lines for simultaneous resonance of the laser (mode m) and the CO_2 Raman-shifted emission (mode m'). (b) High-resolution (20 MHz) spectrum of the Raman emission in pure CO_2 shown in (a).

term in Eq. (9) may be omitted. The mirror phase shifts φ_l and φ_s are determined by the reflective coating used, and their frequency dependence can be calculated. For any pair (m,m') one can then numerically solve the pair of equations (6) and (9) in which the unknowns are the optimal laser frequency and optimal cavity length.

In Fig. 2(a), fulfillment of this double resonance is illustrated for the Raman-shifted spontaneous emission associated with the Q-branch line terminating in the (1 0 0) level of CO_2 with a frequency of $\Delta\bar{\nu}_V = 1388.17$ cm^{-1} [22]. The mirror reflectivity as a function of frequency has been obtained through the measured cavity resonance linewidth and free spectral range (FSR). Superimposed is the computed phase shift $\varphi(\nu)$ incurred at each mirror. Also represented are the calculated (dashed vertical lines) and measured (solid lines) resonance frequencies of the microcavity at double resonance, at which $L = 26.22\ \mu$m and $(m,m') = (61,54)$. A reference laser near ν_l aided in reaching this configuration experimentally before the PDH lock of Fig. 1(a) was engaged. With the pump laser at $\bar{\nu}_l = 11\,539.47$ cm^{-1}, the enhanced spontaneous Raman emission was then observed at $\bar{\nu}_s = 10\,151.40$ cm^{-1} using the spectrometer of Fig. 1(a). For detailed spectral analysis, a scanning Fabry-Pérot interferometer with higher resolution (20 MHz) was used [Fig. 2(b)]. Due to the Q-branch collapse in CO_2, an asymmetric band with $\Delta\nu_R = 270$ MHz without structure is seen [23].

IV. ANALYSIS

To quantitatively compare the measured Purcell-enhanced emission with the expression of Eq. (5), we present the total emission rate as a function of laser frequency for various CO_2 concentrations in air (Fig. 3). These were corrected for the overall detection efficiency of our setup ($\approx 1\%$). The gases were purchased in 100% CO_2 and premixed concentrations of
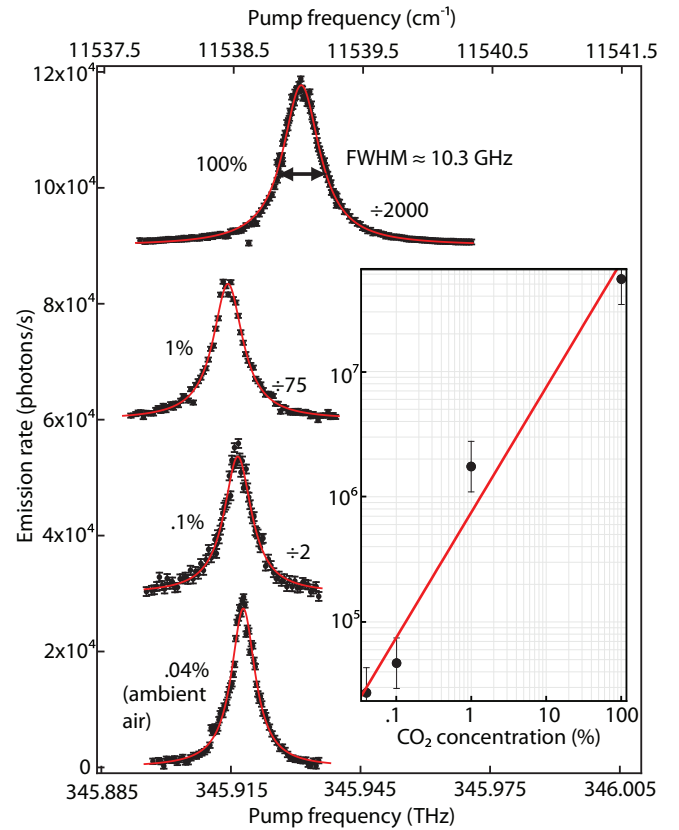
FIG. 3. (Color online) CO_2 Raman photon emission rate as a function of pump laser frequency while maintaining the cavity locked to the pump laser. The traces have been scaled (scale factor indicated near each trace) and offset from each other by 3×10^4 photons/s for clarity. The inset shows the peak emission rate as a function of gas concentration.

1% and 0.1% CO_2 in dry air. The enhancement provided by the cavity is so large that measurements in ambient air can also be comfortably performed. The double-resonance line shapes of Fig. 3 have a linewidth given theoretically by (see Appendix B)

$$\gamma_{\text{cav,DR}}(\nu_l) = \frac{\nu_l}{\Delta\nu_V}\left(\Delta\nu_R + \Delta\nu_c^{(s)}\right), \qquad (10)$$

consistent with observations, given that $\Delta\nu_R = 270$ MHz [Fig. 2(b)]. We believe the dominant error in our measurements is currently associated with the feedback loop illustrated in Fig. 1.

The differential Raman scattering cross section $d\sigma/d\Omega = 4.7 \times 10^{-32}$ cm^2/sr is obtained from the literature [24] after correcting for its frequency dependence. The cavity finesse is also known independently as $\mathcal{F}^{(l)} \approx \mathcal{F}^{(s)} \approx 10\,000$. Thus the total emission rate can be calculated and is represented in Fig. 4(a) as a function of cavity length for various cavity parameters at 100% CO_2 at 760 Torr. The experimental emission rates are represented by the superimposed data. In comparison to a conventional macroscopic resonator of the same finesse, for example $R = 5$ mm and $L = 1$ mm, it is seen that the emission rate is higher by at least a factor of 50, while at the same time employing a sample gas volume reduced by several orders of magnitude. In the absence of the microcavity, the same laser power focused into
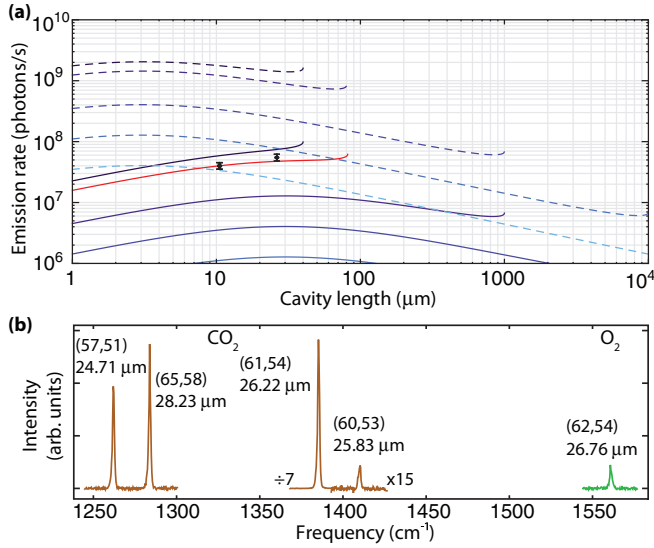
FIG. 4. (Color online) (a) Calculated emission rate [Eq. (5)] for 100% CO_2 at 760 Torr with 10 mW input power as a function of L, for $R = 20\ \mu m$, $40\ \mu m$, $500\ \mu m$, 5 mm, and 50 mm from top to bottom. For the solid (dashed) set of curves, the cavity finesse is 10 000 (100 000). The data correspond to the experimental measurements, and the red line corresponds to the theoretical curve with the same parameters. (b) Raman spectrum constructed by combining Purcell-enhanced emission spectra from different cavity-length–laser-frequency pairs labeled by (m, m') and L.

the same volume as the microcavity would have resulted in only $\gamma_{\text{free},\Delta\Omega} = 2$ photons/s into the same solid angle as that subtended by the microcavity.

The overall enhancement of the Raman emission rate compared to the free-space emission rate into the same solid angle as that subtended by the microcavity can be divided into three contributions (Sec. II). For our current experimental configuration, the greatest contribution (a factor of ≈ 3000) comes from the enhancement of the pump laser intensity due to recirculation at the resonant frequency. It is physically limited only by the mirror losses, i.e., cavity finesse, which may be further increased by several orders of magnitude [25]. The Purcell effect contributes by redirecting the emission into a well-defined spatial mode (a factor of ≈ 170), as well as by enhancing the rate of emission into that mode (a factor of ≈ 40). As seen in Fig. 4(a), the microcavity Purcell enhancement may be further increased by decreasing the length of the cavity and reducing the mirror radius of curvature, so long as $V \gg 1/N$. Also note that if γ_{cav} is exceedingly large, then the effect of stimulated Raman scattering, ignored in Eq. (1), may need to be considered. The Raman gain coefficient can be expressed as $g_s = \gamma_{\text{cav}}/c$ [19]. Therefore, if round-trip cavity losses were to decrease below $g_s L$, then Raman lasing would take place. For 100% CO_2 at atmospheric pressure and with our current experimental parameters, $g_s L \sim 1$ ppm is still significantly less than the current mirror transmission of ≈ 300 ppm and thus stimulated Raman scattering can be safely ignored.

The range of Raman-shifted frequencies that can be observed for a given cavity length and laser frequency pair is of order $\frac{\nu_l}{\Delta\nu_V}\Delta\nu_c^{(s)}$. Nonetheless, conventional Raman spectra

can be constructed based on a set of cavity length and laser frequency pairs which satisfy double resonances for a set of Raman shifts. Such a spectrum is shown in Fig. 4(b), which includes a number of vibrational bands of CO_2 and one of O_2 (100% concentration at atmospheric pressure). Thus the fingerprinting capabilities of Raman scattering are preserved in our scheme.

V. CONCLUSIONS AND OUTLOOK

We have demonstrated the Purcell spontaneous-emission enhancement effect for Raman scattering in gases under ambient conditions. This was achieved by implementing a double resonance in an open fiber microcavity of high finesse by which a large enhancement ($\sim 10^7$) in emission was obtained compared to free space. Good agreement with theory is found for both the absolute emission rate as well as the emission line shape. Since our detection efficiency is only about 1% (a combination of propagation losses, spectrometer losses, and low detector quantum efficiency) and since detection efficiencies of around 20% are routinely achieved with more adequate filters and detectors, it is likely that the approach described here can be used to detect trace gas amounts in the ppm range. Furthermore, the cavity finesse may be increased by at least one order of magnitude [17]. Part-per-billion (ppb) concentrations should be detectable when using resonance Raman scattering, which provides an increase in scattering cross section by several orders of magnitude. With mode volumes of order $\sim 100\ \mu m^3$, such detection would involve few or even one molecule interaction under ambient conditions.

APPENDIX A: CALCULATION OF THE MODE VOLUME FOR MICROCAVITY RAMAN SCATTERING

The effective mode volume that enters the Purcell factor for the case of Raman scattering is given by [10]

$$V = \frac{\int |u_s(\mathbf{r})|^2 d^3r \int |u_l(\mathbf{r})|^2 d^3r}{\int |u_s(\mathbf{r})|^2 |u_l(\mathbf{r})|^2 d^3r}, \qquad (A1)$$

where $u_l(\mathbf{r})$ and $u_s(\mathbf{r})$ are the laser and Stokes spatial mode functions, respectively. The denominator in this expression for the mode volume takes explicitly into account the finite overlap between $u_l(\mathbf{r})$ and $u_s(\mathbf{r})$. The average over the (random) molecular orientations is accounted for in the differential Raman cross section. For a confined Gaussian beam, $u(\mathbf{r}) = [w_0/w(z)]\sin(kz)\exp[-r^2/w(z)^2]$ and the z dependence of the beam spot size $w(z)^2 = w_0^2(1 + z^2/z_R^2)$ as well as the wavefront radius of curvature $R(z) = z(1 + z_R^2/z^2)$ are solely determined by the beam waist w_0 and the Rayleigh range $z_R = \pi w_0^2/\lambda$ [20].

For a planar-concave optical resonator, we have $R = L(1 + z_R^2/L^2)$ and thus $z_R^2 = L(R - L)$. For the numerator

of Eq. (A1), we then calculate

$$\int |u(\mathbf{r})|^2 d^3r = w_0^2 \int_0^L \int_0^\infty \frac{e^{-2r^2/w(z)^2}}{w(z)^2} 2\pi r dr \sin^2(kz)dz$$
$$= \frac{\pi w_0^2}{2} \int_0^L \sin^2(kz)dz = \pi w_0^2 L/4.$$

The denominator of Eq. (A1) is given by

$$\int |u_s(\mathbf{r})|^2 |u_l(\mathbf{r})|^2 d^3r$$
$$= w_{0l}^2 w_{0s}^2 \int_0^L \int_0^\infty \frac{e^{-2r^2[w_l(z)^{-2}+w_s(z)^{-2}]}}{w_l(z)^2 w_s(z)^2} 2\pi r \, dr$$
$$\times \sin^2(k_l z)\sin^2(k_s z)dz,$$

and since $w_s(z)^2 = w_l(z)^2 \lambda_s/\lambda_l$, we get

$$\int |u_s(\mathbf{r})|^2 |u_l(\mathbf{r})|^2 d^3r$$
$$= w_{0l}^2 w_{0s}^2 \frac{\pi/2}{1+\lambda_s/\lambda_l} \int_0^L \frac{\sin^2(k_l z)\sin^2(k_s z)dz}{w_l(z)^2}.$$

We can approximate the z integral by assuming that the function $w_l(z)^{-2}$ varies slowly compared to the harmonic terms such that the integrals over the latter vanish, leaving

$$\int |u_s(\mathbf{r})|^2 |u_l(\mathbf{r})|^2 d^3r$$
$$= w_{0l}^2 w_{0s}^2 \frac{\pi/8}{1+\lambda_s/\lambda_l} \int_0^L w_l(z)^{-2}dz$$
$$= \frac{\pi w_{0s}^2/8}{1+\lambda_s/\lambda_l} \sqrt{L(R-L)} \tan^{-1}\frac{L}{\sqrt{L(R-L)}}.$$

Overall, we then obtain the mode volume of a planar-concave resonator as

$$V = \frac{(\lambda_l + \lambda_s)L^2/2}{\tan^{-1}\frac{L}{\sqrt{L(R-L)}}}.$$

This can be generalized for an arbitrary symmetric resonator of length L to obtain

$$V = (\lambda_l + \lambda_s)\frac{L^2/4}{\tan^{-1}[L/\sqrt{2(R-L/2)L}]},$$

which is the expression of Eq. (4).

APPENDIX B: DOUBLE-RESONANCE LINE SHAPE

In all our experiments, the pump laser of frequency ν_l is locked to a cavity mode with longitudinal mode number m, so

that the double resonance obtained when scanning the laser frequency while collecting the total Raman-scattered light intensity is a convolution of two Lorentzians. One Lorentzian corresponds to the cavity mode with longitudinal mode number m' at frequency $\nu_l - (m - m')$FSR with linewidth $\Delta\nu_c^{(s)}$, where FSR is the cavity free spectral range. The other Lorentzian corresponds to the Raman resonance at frequency $\nu_l - \Delta\nu_V$ with linewidth $\Delta\nu_R$. The line shape of the double resonance is thus equal to

$$\gamma_{\text{cav,DR}}(\nu_l)$$
$$= \gamma_{\text{cav}}A \int_{-\infty}^{+\infty} \frac{1}{(\nu' - (\nu_l - (m-m')\text{FSR}))^2 + (\Delta\nu_R/2)^2}$$
$$\times \frac{1}{[\nu' - (\nu_l - \Delta\nu_V)]^2 + (\Delta\nu_c^{(s)}/2)^2} d\nu',$$

where A is a normalization constant that satisfies

$$A \int_{-\infty}^{+\infty} \frac{1}{\nu'^2 + (\Delta\nu_R/2)^2} \frac{1}{\nu'^2 + (\Delta\nu_c^{(s)}/2)^2} d\nu' = 1,$$

or explicitly $A = \Delta\nu_c^{(s)}\Delta\nu_R(\Delta\nu_c^{(s)} + \Delta\nu_R)/(8\pi)$. Because FSR $\approx c/(2L) = c/(2m\lambda_l/2) = \nu_l/m$, we get

$$\gamma_{\text{cav,DR}}(\nu_l) = \int_{-\infty}^{+\infty} \frac{\gamma_{\text{cav}}A}{[\nu' - (m-m')\nu_l/m + \Delta\nu_V]^2 + (\Delta\nu_R/2)^2}$$
$$\times \frac{1}{\nu'^2 + (\Delta\nu_c^{(s)}/2)^2} d\nu'$$

leading to

$$\gamma_{\text{cav,DR}}(\nu_l)$$
$$= \frac{2\pi\gamma_{\text{cav}}A(1/\Delta\nu_c^{(s)} + 1/\Delta\nu_R)}{[(m-m')\nu_l/m - \Delta\nu_V]^2 + (\Delta\nu_c^{(s)}/2 + \Delta\nu_R/2)^2}$$
$$= \frac{(1/4)(\Delta\nu_c^{(s)} + \Delta\nu_R)^2 m^2 \gamma_{\text{cav}}/(m-m')^2}{[\nu_l - m\Delta\nu_V/(m-m')]^2 + \{m[\frac{\Delta\nu_c^{(s)}}{2} + \frac{\Delta\nu_R}{2}]/(m-m')\}^2},$$

which is a Lorentzian of width

$$\gamma_{\text{cav,DR}}(\nu_l) = m(\Delta\nu_c^{(s)} + \Delta\nu_R)/(m-m')$$
$$= \frac{\nu_l}{\Delta\nu_V}(\Delta\nu_R + \Delta\nu_c^{(s)})$$

as in Eq. (10).

[1] E. M. Purcell, Phys. Rev. **69**, 681 (1946).
[2] P. Goy, J. M. Raimond, M. Gross, and S. Haroche, Phys. Rev. Lett. **50**, 1903 (1983).
[3] R. G. Hulet, E. S. Hilfer, and D. Kleppner, Phys. Rev. Lett. **55**, 2137 (1985).
[4] D. J. Heinzen, J. J. Childs, J. E. Thomas, and M. S. Feld, Phys. Rev. Lett. **58**, 1320 (1987).
[5] K. J. Vahala, Nature (London) **424**, 839 (2003).
[6] J. M. Gérard, B. Sermage, B. Gayral, B. Legrand, E. Costard, and V. Thierry-Mieg, Phys. Rev. Lett. **81**, 1110 (1998).
[7] D. G. Deppe, L. A. Graham, and D. L. Huffaker, IEEE J. Quantum Electron. **35**, 1502 (1999).
[8] F. Cairo, F. De Martini, and D. Murra, Phys. Rev. Lett. **70**, 1413 (1993).
[9] A. Fainstein and B. Jusserand, Phys. Rev. B **54**, 11505 (1996).

[10] X. Checoury, Z. Han, M. El Kurdi, and P. Boucaud, Phys. Rev. A **81**, 033832 (2010).

[11] T. Carmon and K. J. Vahala, Nat. Phys. **3**, 430 (2007).

[12] T. J. Kippenberg, S. M. Spillane, D. K. Armani, and K. J. Vahala, Opt. Lett. **29**, 1224 (2004).

[13] H. Xu, E. J. Bjerneld, M. Käll, and L. Börjesson, Phys. Rev. Lett. **83**, 4357 (1999).

[14] F. Neubrech, A. Pucci, T. W. Cornelius, S. Karim, A. García-Etxarri, and J. Aizpurua, Phys. Rev. Lett. **101**, 157403 (2008).

[15] Y. Colombe, T. Steinmetz, G. Dubois, F. Linke, D. Hunger, and J. Reichel, Nature (London) **450**, 272 (2007).

[16] D. Hunger, T. Steinmetz, Y. Colombe, C. Deutsch, T. W. Hänsch, and J. Reichel, New J. Phys. **12**, 065038 (2010).

[17] A. Muller, E. B. Flagg, J. Lawall, and G. S. Solomon, Opt. Lett. **35**, 2293 (2010).

[18] B. Petrak, K. Konthasinghe, S. Perez, and A. Muller, Rev. Sci. Instrum. **82**, 123112 (2011).

[19] A. Yariv, *Quantum Electronics*, 3rd ed. (Wiley, New York, 1975), p. 466.

[20] H. Kogelnik and T. Li, Appl. Opt. **5**, 1550 (1966).

[21] R. W. P. Drever, J. L. Hall, F. V. Kowalski, J. Hough, G. M. Ford, A. J. Munley, and H. Ward, Appl. Phys. B **31**, 97 (1983).

[22] B. P. Stoicheff, Can. J. Phys. **36**, 218 (1958).

[23] B. Lavorel, G. Millot, R. Saintloup, H. Berger, L. Bonamy, J. Bonamy, and D. Robert, J. Chem. Phys. **93**, 2176 (1990).

[24] W. R. Fenner, H. A. Hyatt, J. M. Kellam, and S. P. S. Porto, J. Opt. Soc. Am. **63**, 73 (1973).

[25] G. Rempe, R. J. Thompson, H. J. Kimble, and R. Lalezari, Opt. Lett. **17**, 363 (1992).